JOURNAL OF GEOPHYSICAL RESEARCH, VOL. 100, NO. D12, PAGES 26,211–26,227, DECEMBER 20, 1995

Diurnal asymmetry of climatic response to increased CO_2 and aerosols: Forcings and feedbacks

Georgiy L. Stenchikov and Alan Robock

Department of Meteorology, University of Maryland, College Park

Abstract. To examine the causes of the observed diurnally asymmetrical climate change over land, the roles of different physical mechanisms are evaluated using a radiative-convective model of the diurnal cycle. This model explicitly calculates a complete set of physical processes, including the water vapor distribution, clouds, transports in the turbulent boundary layer, and convection. Calculations were carried out for midlatitude summer and winter and for tropical spring conditions taking into account the most important climate forcings: CO_2 increase, tropospheric aerosol pollution, and the combined case with simultaneous CO_2 and aerosol effects. We find that feedbacks in the climate system are more important than forcings in producing diurnal asymmetry. The water vapor shortwave feedback dominates the diurnal distribution of the response. For all cases with warming, the diurnal temperature range (DTR) decreases, not due to the greenhouse effect of water vapor, but as a result of more intensive absorption of the solar radiation in the near infrared by water vapor and cloud water in a warmer, wetter climate independent of the type of forcing. Aerosol reflection and absorption of solar radiation cool the surface and decrease DTR directly, but the negative daytime water vapor feedback virtually cancels out the diurnal asymmetry. In the combined case, with a 50% CO_2 content increase combined with tropospheric aerosol pollution, which is not far from the current observed conditions over land, the greenhouse warming raises the temperature enough that the direct aerosol effect decreases the DTR. In all cases the time and spatial redistribution of clouds have a significant impact on the climate sensitivity and diurnal cycle. As in the observations, increasing of cloudiness and water vapor content occurs with decreasing of the DTR. In our model the cloudiness and water vapor changes are produced by the same forcings that lower the DTR; they are not independent causes of changes of the DTR, but rather are important internal feedback mechanisms.

Introduction

It has been observed [*Karl et al.*, 1991, 1993; *Folland et al.*, 1992], by using the daily maximum and minimum temperature data sets archived since World War II, that global warming over a large part of the land surfaces has been accompanied by statistically significant decreasing of the diurnal temperature range (DTR), as well as increasing of the cloudiness fraction. The observed increase of the diurnally average temperature is produced mainly by the increase of the minimum nighttime temperatures. Daily maximum temperatures have increased much more slowly and have even decreased in some places. These diurnally asymmetrical changes can significantly influence agriculture, transport, communications, and other human activities. Gaining understanding of these changes cannot only help us to predict the effects of climate changes on these activities, but also can help to improve our understanding of the mechanisms of climate variations.

This change of the diurnal cycle is a very important characteristic of climate change, but its causes are not well understood [*Karl et al.*, 1993]. Energetically, the change of the shape of the diurnal cycle is a second-order effect in comparison with the change of the diurnal mean temperature. It is reasonable to anticipate that the most powerful radiative forcings for the diurnal mean temperature, provided by greenhouse gases and aerosol pollution of the atmosphere, can also have significant impacts on the diurnally asymmetrical component. In discussing surface temperature sensitivity we consider the radiative forcing from these changes near the surface, rather than at the top of the troposphere.

It is important to distinguish between diurnally asymmetrical forcings of the climate system, and diurnally asymmetrical feedbacks. For example, while aerosols clearly have a diurnally asymmetrical forcing, reducing the radiation that reaches the surface during the day and slightly increasing the downward thermal radiation at night, feedbacks may produce an unanticipated equilibrium response to this forcing, with as much cooling at night as during the day. In this paper we investigate both forcings and feedbacks, and find that feedbacks are as important.

There have been only a few climate model calculations that have investigated this problem. General circulation model (GCM) calculations of diurnal cycle response to carbon dioxide doubling by *Rind et al.* [1989] and *Cao et al.* [1992] and transient CO_2 and tropospheric aerosol increases by *Hansen et al.* [1993] all produced DTR reductions, but with large differences from the observations. A GCM is so complex, and for a particular location includes changes in advective forcings as well as physical processes in the

Copyright 1995 by the American Geophysical Union.

Paper number 95JD02166.
0148-0227/95/95JD-02166$05.00

vertical, that it is difficult to figure out the reasons for the DTR changes. For this reason, Cao et al. utilized a radiative-convective model (RCM) to diagnose their GCM results, and we take the same approach in this paper. Rind et al. ignore the effects of CO_2 and water vapor on shortwave radiation, giving an incomplete explanation for the modeled DTR reductions. While Hansen et al. correctly attribute the DTR reductions to increased water vapor, aerosols, and clouds, they do not separate these effects and investigate their relative importance.

Recently, *Hansen et al.* [1995] have used their Wonderland GCM [*Hansen et al.*, 1993] to further investigate the causes of diurnal asymmetry of climate change. They provide a very nice analysis of the importance of cloud feedbacks, which, in combination with aerosols and greenhouse gases over land are needed to produce the observed asymmetry but do not focus on the water vapor-shortwave radiation feedback. Their model, however, does not produce the needed cloud changes interactively, and they discuss them as an externally imposed forcing. They point out that the cloud changes could be a feedback caused by sulfates, but their model does not include this level of complexity.

RCM experiments with CO_2 doubling [*Cao et al.*, 1992] successfully showed that absorption of solar radiation by CO_2 and water vapor, together with boundary layer feedbacks, tends to decrease DTR, but they did not separate these effects. Furthermore their experiments were carried out for only one restrictive equinox climatic condition with prescribed zero advective fluxes, prescribed relative or absolute humidity, and prescribed cloud cover. Calculations with a dry RCM [*Veltishchev and Demchenko*, 1993] also showed a decrease of DTR with increased CO_2, but they attributed the cause to increased thermal emission of the warmer daytime surface. Without a water vapor feedback and with a coarse vertical structure, this effect was probably amplified due to lack of increased water vapor emission of thermal flux from the atmosphere.

In this paper we try to understand the discrepancy between theory and observations by reevaluating the CO_2 and tropospheric aerosols forcings and feedbacks from the viewpoint of their influence on the shape of the diurnal cycle. We exploit a newly developed RCM of the diurnal cycle (described in the Appendix) with an entire set of local physical processes internally generated by the model, which is able to reproduce climatic thermal equilibrium regimes of the land-atmosphere system accounting for the diurnal cycle, cloud variations, turbulence, and boundary layer processes. Previous RCMs have not been able to describe all these processes and therefore were unable to completely investigate diurnal cycle sensitivity.

In order to calculate the effects of CO_2 and aerosol changes on the diurnal cycle, we ran the model for three cases: midlatitude winter, midlatitude summer, and spring in the tropics. By specifying only the location, time of year, net radiation at the top of the atmosphere (which is equivalent to the convergence of energy by advection in the column), and surface albedo and wetness, the model internally generates the equilibrium climate, including the water vapor and cloud distributions. The parameters for our three cases are shown in Table 1. In accordance with observations over land [*Peixoto and Oort*, 1992], in the tropics and in midlatitude summer the atmospheric column loses 40 W/m^2 and 100 W/m^2, respectively, but in winter receives 110 W/m^2, and the other parameters were chosen to be representative. It is worth emphasizing that these advective sources over land are defined not only by equator-to-pole energy transport but also by zonal land-ocean energy exchanges. Zonal mean data, which traditionally are used to estimate these terms, can give substantial mistakes over land.

Table 1. Parameters for the Three Cases

	Midlatitude Summer	Midlatitude Winter	Tropical Spring
Latitude, °N	45	45	15
Month	June	Jan.	April
Column energy convergence, W/m^2	−100	110	−40
Surface albedo	0.17	0.35	0.17
Surface wetness	0.1	1.0	0.5

The calculated radiative balance at the top of the atmosphere automatically corresponds to the imposed observations, with an discrepancy of less than 0.05 W/m^2. For these calculations, we use a 12-layer version of the RCM with the same vertical grid as in the NCAR CCM1 GCM [*Williamson et al.*, 1987] to have the possibility for comparisons with GCM calculations.

The most important human impacts on the atmosphere in the past century have been inputs of greenhouse gases and aerosols. Greenhouse gases have long lifetimes and are well mixed in the atmosphere, but aerosols, especially in the troposphere, have relatively short lifetimes and are distributed mainly over land, and very nonuniformly in altitude and horizontally. In some regions over land, tropospheric aerosols and CO_2 may cause comparable radiative forcings, but with an opposite sign [*Charlson et al.*, 1992; *Kiehl and Briegleb*, 1993]. Of course, on a local and even regional basis, land surface modifications by humans can also be important causes of climate change, and our model is well suited to studying them, but in this paper we look at only two human-induced forcings, changes of CO_2 (as a surrogate for all greenhouse gases) and changes of tropospheric aerosols. We present calculations for doubled CO_2, increased tropospheric aerosols with a typical optical depth of ~0.2, and a combination of 50% increase in CO_2 with the aerosol increase. (An experiment with a 1% increase of the solar constant, which provides a very clear initial forcing, was performed for comparison.) We use "average continental aerosol" [*D'Almeida et al.*, 1991], with optical properties as shown in Table 2. Average continental aerosol is mostly sulfate aerosol, but is slightly contaminated by dust and soot, which increase its absorption in the visible band. For the boundary layer this contaminated sulfate aerosol is physically more reasonable than pure sulfate aerosol. The aerosol is distributed with a constant mixing ratio in the lowest two layers (~2 km) of the model [*D'Almeida et al.*, 1991].

The experiments presented here should be considered as illustrative and the exact magnitude of the results considered as approximate, but the qualitative conclusions are of general interest. We arbitrarily chose three climatic regimes to illustrate our points, but just as easily could have balanced the model at other locations and times of year. Furthermore, we run the model to equilibrium with constant convergence of energy in the column and no large-scale vertical motion. We do this to isolate the important radiative and surface feedbacks

Table 2. Aerosol Optical Properties

	Wavelength, μm			
	0.3 - 0.45	0.45 - 0.75	0.75 - 4	4 - 250
Extinction coefficient, g/m^2	2.70	0.90	0.04	0.03
Single scattering albedo	0.95	0.95	0.60	—
Asymmetry factor	0.65	0.60	0.40	—

that influence the diurnal cycle, but realize that imposing more realistic time-dependent boundary conditions or including feedbacks not now in our model might produce different results. The effects of these other factors will require further study that is beyond the scope of the present paper.

First we describe the diurnal cycles of the forcings due to CO_2 and aerosols. Next we present the results of the response to doubling CO_2 with our model and an explanation of the feedbacks responsible for the diurnal asymmetry. Then a theoretical analysis of the response of the diurnal cycle of surface temperature is given, to further explain the reactions of the diurnal cycle to an oscillatory forcing. Finally, the results of aerosols and aerosols combined with increased CO_2 are described.

Diurnal Cycle of Forcing Due to CO_2 and Aerosols

Carbon dioxide intensively absorbs infrared (IR) radiation and also has a much weaker, but not negligible, absorption band in near-infrared (NIR) solar radiation. In spite of its small value, the NIR absorption by CO_2 results in a diurnal asymmetry of the downward shortwave radiation that is the same size as the diurnal asymmetry of the downward longwave radiation. Tropospheric aerosols have a large extinction coefficient in visible radiation and very weak absorption in the IR. So both of these optically active components affect both the solar and thermal radiative fluxes and the net forcings are the combination of short- and longwave effects. The diurnal variation of solar flux is very strong in comparison with the thermal flux, so the diurnal asymmetry of CO_2 forcing, defined mainly by IR effects, is much smaller than that due to aerosols, which is defined mainly by the scattering and absorption of the diurnally asymmetrical solar radiation.

Shortwave forcing will of course correlate with insolation, decreasing the downward solar radiation most at noon. The downward IR fluxes depend on atmospheric temperature, so the IR forcings will be in phase with the diurnal oscillations of the atmospheric temperature, making the thermal radiation reaching the surface during the daytime larger than at night. The amplitude of this diurnal cycle will depend on the average height of the downward radiating layer, as the amplitude of the diurnal wave of temperature decreases rapidly with height, and on the opacity of the layers between the radiation layers and the surface. Cloud variations would of course be the most important determinant, as they are essentially black-body radiators, while CO_2 has a much lower emissivity. Assuming that clouds do not change, however, the warmer climates (with a larger atmospheric loading of water vapor in the lower layers) would be expected to produce a slightly smaller diurnal asymmetry of downward longwave radiation, as the diurnal cycle of downward radiation from the CO_2 would be absorbed more by the water vapor, making the surface less sensitive to CO_2 variations.

The net effect, therefore, of increased CO_2 would be to increase the downward longwave radiation but to decrease the downward shortwave radiation, due to the NIR absorption band. The diurnal asymmetry of the downward longwave radiation would be smaller than that of the shortwave, producing a forcing with warming at night and a small net warming or cooling during the day, depending on the climatic regime (Table 3). We doubled the CO_2 for the equilibrium climates for the three regimes described above (Table 1), and present in Figure 1a the instantaneous change in the downward fluxes for the current climate, before the climate can react to the doubled CO_2. The reduction of downward shortwave is approximately the same in all three cases, but is slightly more in the summer case due to more solar insolation. The downward IR effect, on the other hand is much more diurnally uniform for all three cases, and the total effect is smaller in the regions with more lower atmosphere water vapor. Because there is a diurnal cycle of cloudiness in all three cases, the short- and longwave forcings also show their effects. This is particularly evident for the winter downward IR, which has no clouds in the afternoon, while the other two cases remain overcast but with only thinner afternoon clouds.

The aerosol forcings are illustrated in Figure 1b and in Table 3. Clearly the longwave effects are minuscule, and the shortwave effects produce large cooling in the daytime. The winter afternoon shortwave reduction only approaches the summer and tropical ones because of the lack of clouds (see

Table 3. Diurnal Cycles of Forcings Due to Increased CO_2 and Aerosols

Forcing	Shortwave Effect	Longwave Effect	Net Effect
Increased CO_2	Small daytime cooling	Small warming, very slightly larger during the day	Warming at night, small cooling to small warming during the day
Increased aerosols	Large daytime cooling	Very small warming, slightly larger during the day	Large daytime cooling

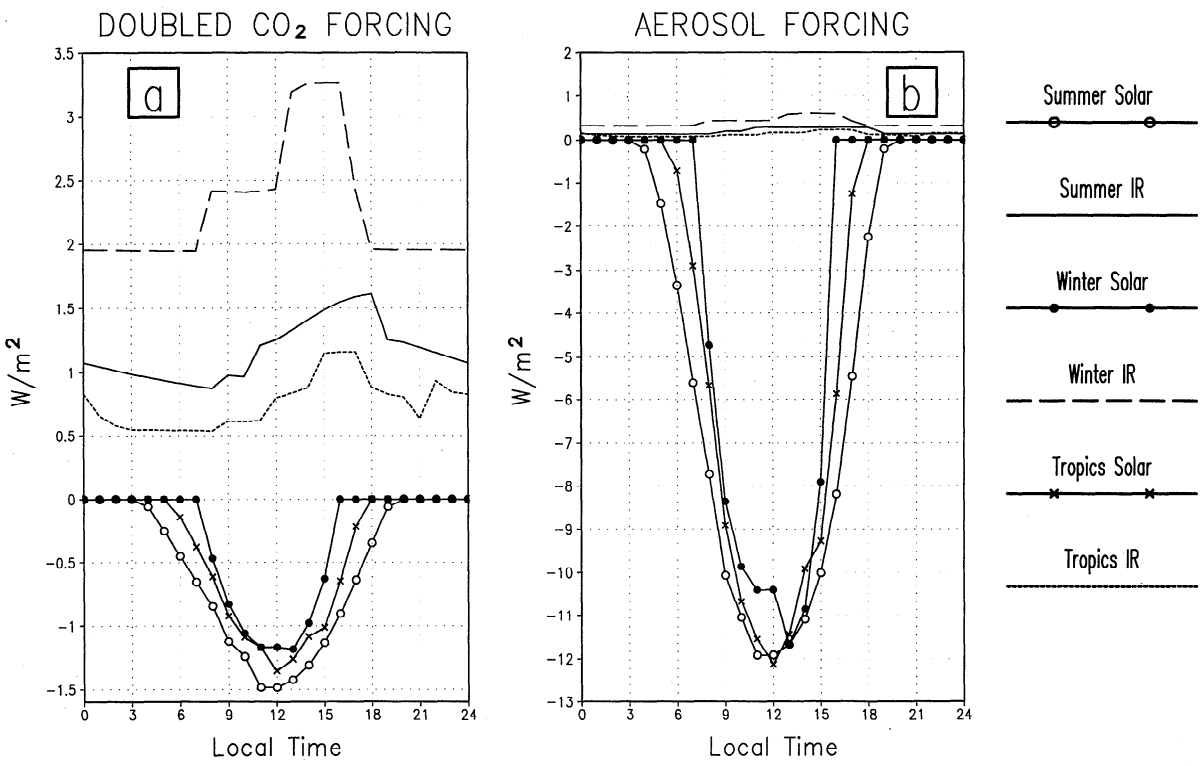

Figure 1. Diurnal distribution of the radiative surface forcings for the three cases due to (a) CO_2 doubling and (b) tropospheric aerosol pollution.

Figure A1, described in the Appendix) and the lower solar declination.

So both CO_2 and aerosol forcings produce less warming in the daytime than at night! (Of course, the diurnal asymmetry of the aerosol forcing is much larger.) Therefore, if the climate system responded instantaneously and with no feedbacks, either CO_2 increases or aerosol increases, but especially their combination, would produce the observed diurnal asymmetry of climate change. The climate system is not that simple, as we shall see, and in fact it will turn out that diurnally asymmetrical nonlinear responses of the climate system completely dominate the final response, independent of the diurnal asymmetry of the forcing.

It turns out that the precise timing of the forcings in the diurnal cycle is very important: the forcing and response are shifted in time with respect to each other, so the phase of the forcing is crucial to understand how it influences the DTR. Solar forcings, which are practically in phase with diurnal insolation, in most cases are a more important cause of DTR change than IR forcings, which are smaller and mainly in phase with the surface temperature variation. This simple but important point we will explain later, illustrated by the results of calculations.

The resulting changes depend on the reaction of all the elements of the nonlinear climate system and, as it is well known, feedbacks may be more important than initial forcings. A good example is the water vapor feedback in diurnal average greenhouse warming, which amplifies the effect significantly due to additional downward IR emission [*Manabe and Wetherald*, 1967; *Ramanathan and Coakley*, 1978]. Moreover, it has been observed that decreasing of DTR correlates with increasing of clouds, and it is clear that even a time redistribution of clouds may cause strong diurnal asymmetrical effects. So it is important to account for the effects of clouds on climate sensitivity and DTR.

Diurnal Cycle of Response to Doubled CO_2

Figure 2a shows the changes of the diurnal average vertical temperature structure as a result of CO_2 doubling for all cases, including a 1% increase of solar constant with interactive clouds. The warmer climates (in the tropics and in summer) exhibit larger sensitivities due to a larger water vapor greenhouse feedback. The warming increases in altitude in the troposphere for all cases except winter due to the water vapor and lapse rate feedbacks, as discussed by *Schneider and Dickinson* [1974] and *Lindzen et al.* [1982]. In winter the warming is practically uniform in the lower and middle troposphere and decreases in the upper troposphere. CO_2 doubling produces cooling in the stratosphere, in contrast with the solar constant experiment. The lower summer sensitivity in comparison with the tropics is connected with the lower prescribed surface wetness, which limits the water vapor feedback. The strong gap in the warming for the summer case between 200 and 300 mbar is caused by the formation of a new layer cloud in this region at the end of the night.

The diurnal cycle of surface temperature response to doubled CO_2 is shown in Figure 2b. Experiments without cloud feedbacks, keeping clouds fixed at their equilibrium $1xCO_2$ diurnal average values are also shown. A significant decrease of the diurnal range is observed in all cases, especially in summer and in the tropics. Even in the experiment with a 1% increase of solar constant, when the forcing is very simple and would tend to increase DTR,

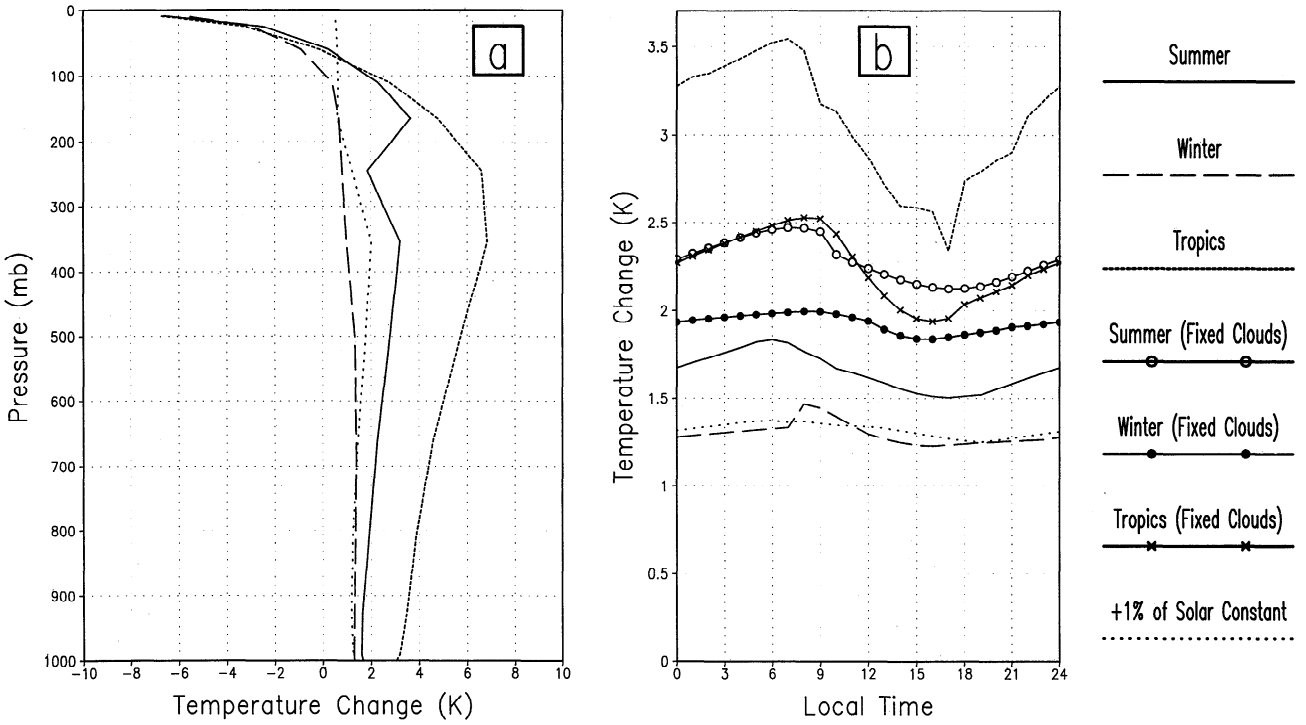

Figure 2. Equilibrium temperature response to doubling of CO_2 for (a) diurnal mean vertical distribution and (b) surface temperature for midlatitudes in summer and winter and the tropics in spring. Unmarked curves are for the full model with interactive clouds. For comparison, results are also shown for results with fixed clouds for CO_2 doubling and for the full model with a 1% solar constant increase.

powerful feedbacks actually decrease it. The warmer climates (summer and tropics cases) also exhibit larger DTR reductions. For the fixed cloud cases, the warmer climates produce a larger diurnal average temperature change, as would be expected due to a larger positive water vapor-greenhouse feedback. They both also exhibit, however, a greater reduction of DTR, which is mostly due to a larger negative daytime water vapor-shortwave feedback.

Clouds produce both positive and negative feedbacks, depending on the climatic regime. Although the modeled clouds show qualitatively and quantitatively reasonable behavior, the results depend on the way clouds are parameterized, and the results here should be taken as illustrative, but by no means definitive. For the tropics, clouds enhance the diurnal average warming, and enhance the DTR asymmetry. In the midlatitudes they reduce the diurnal average warming and have minimal effects on the DTR asymmetry. The reasons for these effects are explored in detail in the next two sections, addressing feedbacks with surface fluxes, water vapor, and clouds.

Water Vapor and Surface Flux Feedbacks

When CO_2 is doubled and the system reaches a new equilibrium, various feedback processes act to modify the initial radiative forcing. In Figures 3-5 we present these equilibrium changes of all radiative fluxes at the surface as well as latent and sensible heat fluxes. To emphasize the cloud effects, the interactive and fixed-cloud feedbacks are presented for each climate regime. In the daytime, at the surface a large reduction of sensible heat flux tends to be compensated by a larger increase of latent heat flux. The latent heat flux increases exponentially with temperature due to the Clausius-Clapeyron relation, but the compensating sensible heat flux reduces linearly with temperature [*Cao et al.*, 1992]. The sum of these feedbacks has approximately the same order as the direct absorption of the solar radiation by CO_2 (Figure 1a). Surface cooling for each of these mechanisms at noon is not more than about 2 W/m^2 for the midlatitude calculations, but in the tropics this feedback is somewhat larger. In the daytime and nighttime, the downward IR flux increases due to the combined greenhouse effects of increased water vapor and CO_2 together with increased atmospheric temperature. Because this increase is slightly larger in the daytime, it tends to increase DTR. The change of upward thermal flux does not have a substantial diurnal cycle. The larger temperature increase at night results in about the same change in upward IR flux as the smaller temperature increase from a warmer surface during the day, due to the fourth-power relationship of the Stefan-Boltzmann law.

A more powerful feedback, and the one which is mainly responsible for the asymmetry of the diurnal cycle of the warming, is the increase of absorption of solar radiation in the NIR by water vapor. This effect is particularly evident in the calculations with fixed clouds, and reaches 4-6 W/m^2 at noon. It is smaller in the winter when there is a smaller change in water vapor, and the winter therefore has a smaller diurnal asymmetry.

Cloud Feedbacks

Clouds influence the entire solar spectrum, and their redistribution and cloud water increase produce flux changes

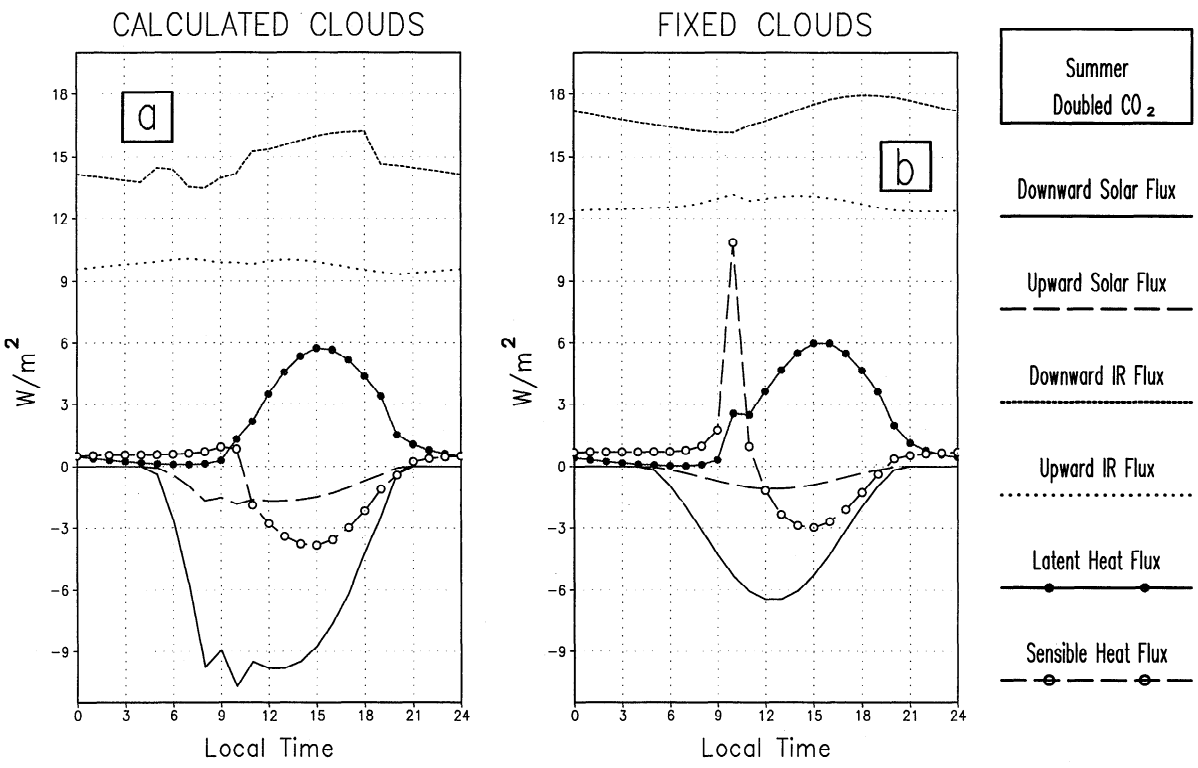

Figure 3. Changes of all surface flux components for CO_2 doubling in midlatitude summer for (a) interactive clouds and (b) for fixed clouds.

of up to 30-60 W/m^2 in winter and in the tropics, but only 3-4 W/m^2 in summer when daytime clouds do not change (Figures 3-5). This last value gives an estimation of the cloud water feedback. In all cases, changing clouds produce much larger changes in downward shortwave and IR fluxes than do fixed clouds, but they compensate. In the tropics, the shortwave dominates, but in winter they are almost the same.

The diurnal average value and amplitude of the response are very different for the cases with calculated and fixed clouds (Figure 2b). With fixed clouds the responses in different seasons are much closer to each other, which confirms the observational and model evidence of the important role of clouds in DTR changes. The cloud diurnal cycles and changes in solar and IR heating rates for the three cases with doubled CO_2 are shown in Figure 6. (The corresponding distributions for the base regimes are shown in Figure A1 in the Appendix.).

Cloud changes can affect the model climate due to time or vertical redistribution, change of the mean cloud fraction, or change of cloud water content. In winter (Figure 6a), new clouds occur in the layer 700-850 mbar from 0700 until 1300, shortening the clear sky period in the daytime. Increased IR cooling corresponds to these changes very closely, due to larger thermal emission by the optically thick clouds. In the lower layer (850-1000 mbar) the IR heating rates increase (cooling rates decrease) due to lifting of the cloud top. The changes in heating rates are substantial and reach 25% of the base values.

In summer (Figure 6b), the distribution of the convective clouds does not change, but at the end of the night a stratiform cloud forms in the upper troposphere, which increases the IR cooling above the cloud and decreases it below the cloud.

In the tropics (Figure 6c), the main change is lifting of the cloud tops from slightly below 400 mbar to 300 mbar in the night, morning, and evening. This again increases the IR cooling near the tropopause and decreases it in the middle and lower troposphere, due to decreasing of the cloud-top temperature.

In all cases increased solar heating rates are connected with stronger absorption of the NIR solar radiation by the warmer and moister atmosphere, as well as increased NIR absorption by the increased CO_2.

As for the surface temperature response (Figure 2b), the tropical and summer cases show approximately the same sensitivity in experiments with fixed clouds. But when clouds were calculated prognostically by the model, cloud feedbacks increase the diurnal averaged sensitivity for the tropical case, as the top of the clouds lifted, but in the midlatitudes clouds decrease the sensitivity both in summer and in winter. In contrast to this behavior, in all cases cloud feedbacks increase the relative (in comparison with diurnal average warming) change of the DTR.

So cloud effects are variable and they have different signs in different regimes, that is, in different regions. Therefore averaging cloud feedbacks over a large area, a hemisphere for example, would give a very poor representation of regional cloud effects.

Phasing and Amplitude of Forcing and Response

In order to explain the above results and to better understand the interplay between forcings and feedbacks, we conducted a theoretical analysis of the timing and phasing of

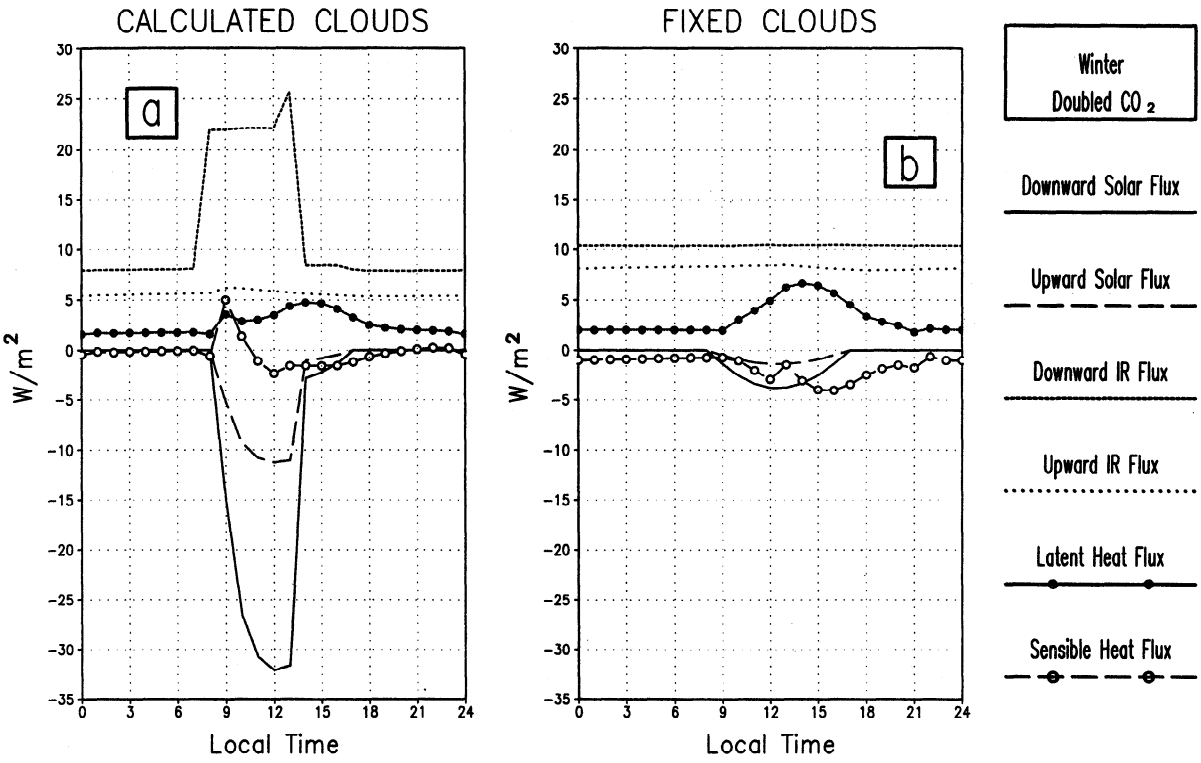

Figure 4. Same as Figure 3, but for midlatitude winter.

changes of fluxes and temperature in a simplified diurnal cycle.

The timing of the forcings and feedbacks is very important to understand their effects on the DTR, due to the time-dependent oscillatory nature of the diurnal cycle and the finite thermal capacity of the soil. There are two main types of disturbances of the energetic regime of the surface. The IR downward flux is changing in phase with temperature variations, but the solar flux is synchronized with the insolation (Figures 3-5). The time dependence of the sensible

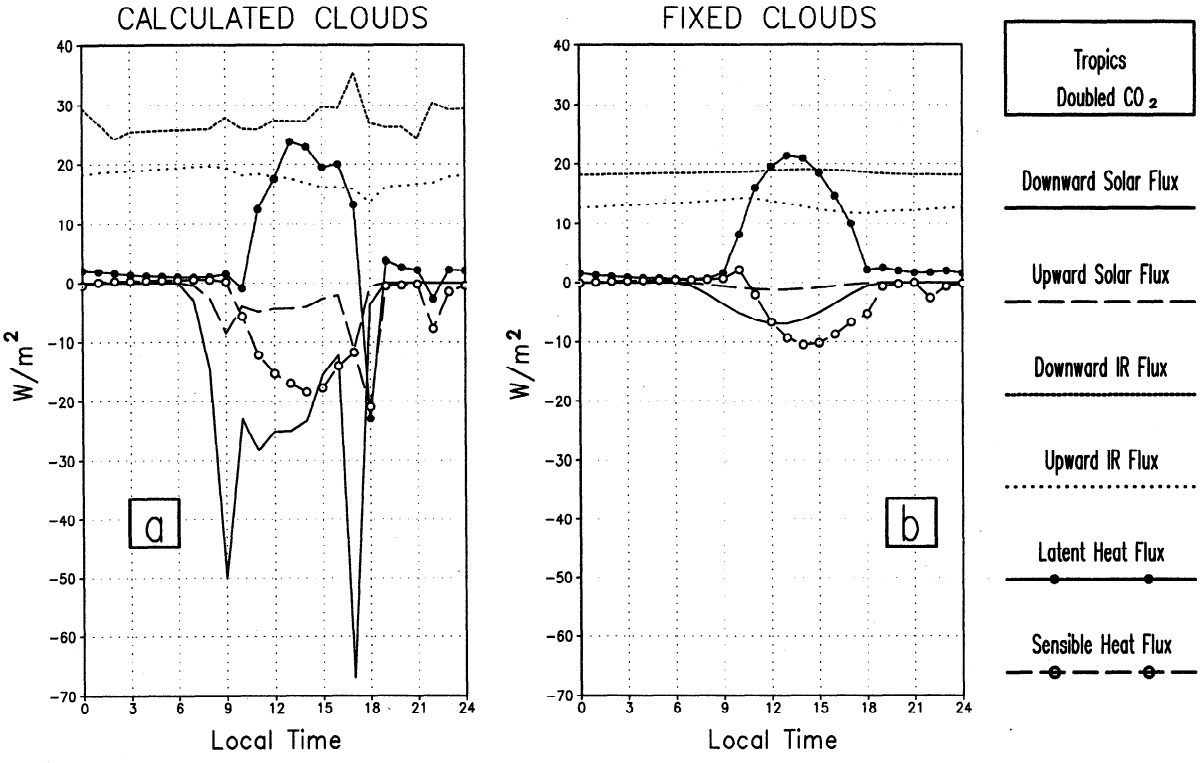

Figure 5. Same as Figure 3, but for tropics spring.

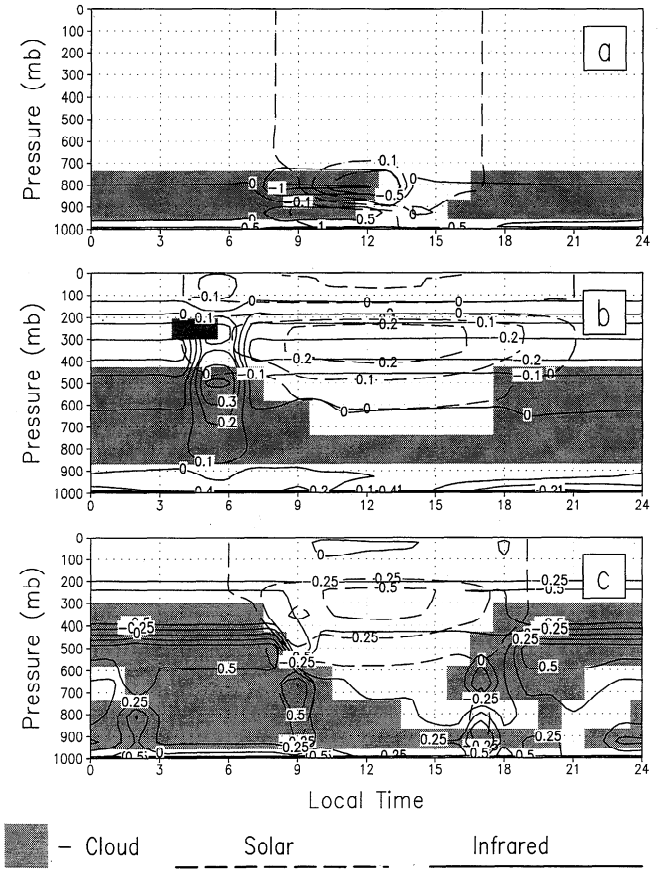

Figure 6. Final equilibrium diurnal distribution of clouds and change of radiative heating rates due to CO_2 doubling for (a) midlatitude winter, (b) summer, and (c) tropics spring. See Figure A1 to compare to control cloud distributions and heating rates.

and latent heat fluxes is more complicated, but they do not contribute much.

In the time-dependent, equilibrium, diurnal cycle solution, the response of the surface temperature is shifted relative to the phase of surface forcing, due to the finite soil thermal capacity. To clarify the role of the different diurnally asymmetrical forcings and feedbacks in the DTR change, let us discuss the evolution of the ground temperature separately, considering the calculated feedbacks (Figures 3-5) as external forcings for the surface and taking only the thermal emission of the ground as a stabilizing mechanism. For simplicity's sake, we use ground temperature for our analytical solution, rather than air temperature of the lowest layer, but surface air temperature for our calculated regimes is close to the ground temperature and has a very close phase. The air temperature may be different in some cases with very low turbulence and very high stability over snow [*Groisman et al.*, 1994], but this was not important in any of the cases here.

For the undisturbed case, let us separate the ground temperature T_g into the mean T_o and oscillatory parts $T_c(t)$

$$T_g = T_o + T_c(t) \tag{1}$$

so that the integral of the oscillatory part over the period of a day τ vanishes:

$$\int_0^\tau T_c(t)dt = 0. \tag{2}$$

Then the equation for diurnal variations of the temperature may be written in the form, where we take into account that $T_c \ll T_o$,

$$c_g \frac{dT_c}{dt} = -F_L - F_S + (1-\alpha)S\downarrow + I\downarrow - \sigma T_o^4\left(1+\frac{4T_c}{T_o}+\frac{6T_c^2}{T_o^2}\right) \tag{3}$$

where c_g is the thermal capacity of the soil layer, F_L and F_S are the latent and sensible heat fluxes, $S\downarrow$ and $I\downarrow$ are the downward solar and IR fluxes, and α is the surface albedo. The last term describes the thermal emission of the surface according to the Stefan-Boltzmann law. The diurnal cycle of the temperature change (ΔT_c) is determined by the following equation:

$$c_g \frac{d\Delta T_c}{dt} = -\Delta F_L - \Delta F_S + (1-\alpha)\Delta S\downarrow + \Delta I\downarrow - \sigma T_o^4\left(\frac{4\Delta T_c}{T_o}+\frac{12T_c\Delta T_c}{T_o^2}\right). \tag{4}$$

ΔT_c can also be separated into the diurnal average ΔT_o and diurnally asymmetrical oscillatory part T_a, which is a function of time t and has zero average value. ΔT_o is determined by the diurnal average energy balance, by averaging (4) over time (designated by the bar) and assuming that $T_a \ll \Delta T_o$ and $T_c \ll T_o$:

$$\overline{-\Delta F_L - \Delta F_S + (1-\alpha)\Delta S\downarrow + \Delta I\downarrow} - 4\sigma T_o^3 \Delta T_o = 0 \tag{5}$$

The evolution of the diurnally asymmetrical oscillatory part T_a is then described by

$$c_g \frac{dT_a}{dt} = F_{SUN} + F_{IR} - 12\sigma T_o^2 T_c \Delta T_o - 4\sigma T_o^3 T_a \tag{6}$$

where F_{SUN} and F_{IR} are the remaining oscillatory parts of the surface forcings which are synchronized with insolation and temperature variations, respectively. Taking the first harmonics of the Fourier transformations of these forcings and surface temperature $T_c(t)$,

$$F_{IR} = -A_o \sin\frac{2\pi t}{\tau}$$
$$F_{SUN} = B_o \sin\left(\frac{2\pi t}{\tau}-\frac{\pi}{2}\right) \tag{7}$$
$$T_c = -C_o \sin\frac{2\pi t}{\tau}$$

with amplitudes A_o, B_o, and C_o, which can be evaluated from the results of calculations, transforms (6) to the form:

$$c_g \frac{dT_a}{dt} = B_o \sin\left(\frac{2\pi t}{\tau}-\frac{\pi}{2}\right) - A_o \sin\frac{2\pi t}{\tau} + 12\sigma T_o^2 C_o \sin\frac{2\pi t}{\tau}\Delta T_o - 4\sigma T_o^3 T_a. \tag{8}$$

The first term of the solution, starting from the initial condition $T_a(0) = 0$,

$$T_a = \frac{\tau}{2\pi c_g}\left[-B_o\cos\left(\frac{2\pi t}{\tau}-\frac{\pi}{2}\right)+A_o\cos\frac{2\pi t}{\tau} - 12\sigma T_o^2 C_o \Delta T_o \cos\frac{2\pi t}{\tau} + \left(12\sigma T_o^2 C_o \Delta T_o - A_o\right)\exp\left(-\frac{4\sigma T_o^3}{c_g}t\right)\right], \quad (9)$$

describes the effect of solar forcings, the second, atmospheric IR and boundary layer effects; the third, thermal emission from the surface, and the last, the eigen solution, which goes to 0 as $t \to \infty$. Evaluating the diurnal asymmetry, using (9) for summer, for example, we get a reasonable value of the order of 0.25 K.

The relative role of different effects is defined by the parameters characterizing the amplitude of the different terms, and with figures corresponding, for example, to the summer case:

$$B_o \approx 5;\ A_o \approx 2;\ 12\sigma T_o^2 \Delta T_o C_o \approx 1 \quad (10)$$

shows that solar effects are at least two times more significant than IR effects and thermal emission from the surface produces the smallest diurnal asymmetry. In winter and in the tropics, the solar effects are even more significant.

The solution (9) also shows that the surface temperature response is shifted by a quarter of the period (6 hours) in comparison with forcing. Solar forcing, which has its minimum exactly at noon, decreases the daytime maximum and increases the nighttime minimum temperatures. The IR atmospheric forcing increases the temperature at midnight, when T_c has not yet reached a minimum, and decreases it at noon, when T_c has not reached its maximum. So the solar forcings are the most important cause of diurnal asymmetry.

In contrast, *Veltishchev and Demchenko* [1993] claim that surface emission feedback is the main cause of diurnal asymmetry, but our analysis shows that this effect is small due to both a small amplitude and the wrong phase; it increases the temperature at noon and decreases it at midnight. Their conclusion is due to the absence in their model of water vapor effects and a stationary interpretation of the surface temperature response.

Aerosol Effects on the Diurnal Cycle

To investigate the contribution of aerosols to the change of DTR, calculations for different aerosol optical depths and for the combined case of simultaneous 50% CO_2 increase and aerosol pollution were carried out, as described in the second section. The changes of surface temperature due to aerosol pollution with optical depth 0.216, with interactive and fixed diurnal-average clouds, are shown in Figure 7a, and the combined effects of 50% CO_2 increase with aerosols are shown in Figure 7b.

For aerosols only (Figure 7a), the diurnal average effect is cooling for all cases, except for the tropics with interactive clouds. In all the cases with fixed clouds, aerosols produce cooling, with slightly more cooling during the day (a decrease of the DTR), as expected due to the aerosol forcing (Figure 1b). There is actually very little change of DTR, and the water

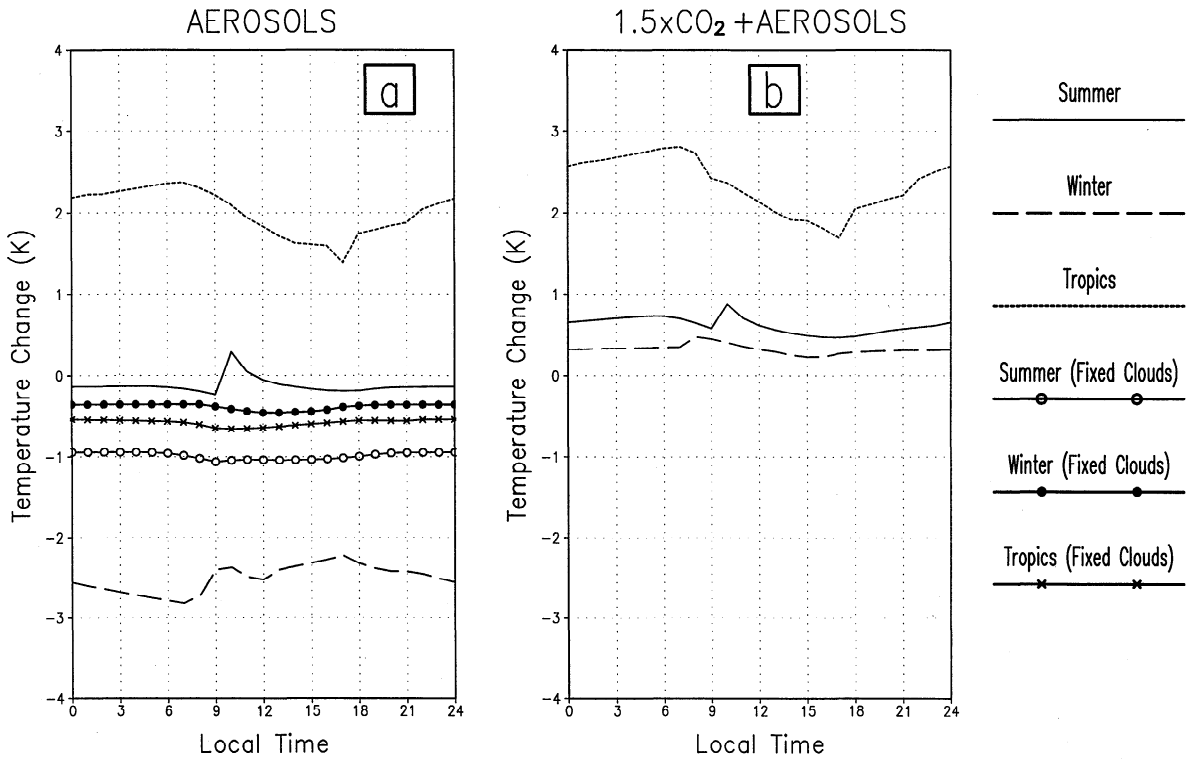

Figure 7. Equilibrium surface temperature response to adding average continental aerosol with optical depth 0.216 with (a) interactive and fixed clouds, and (b) the same for aerosols combined with a 50% CO_2 increase.

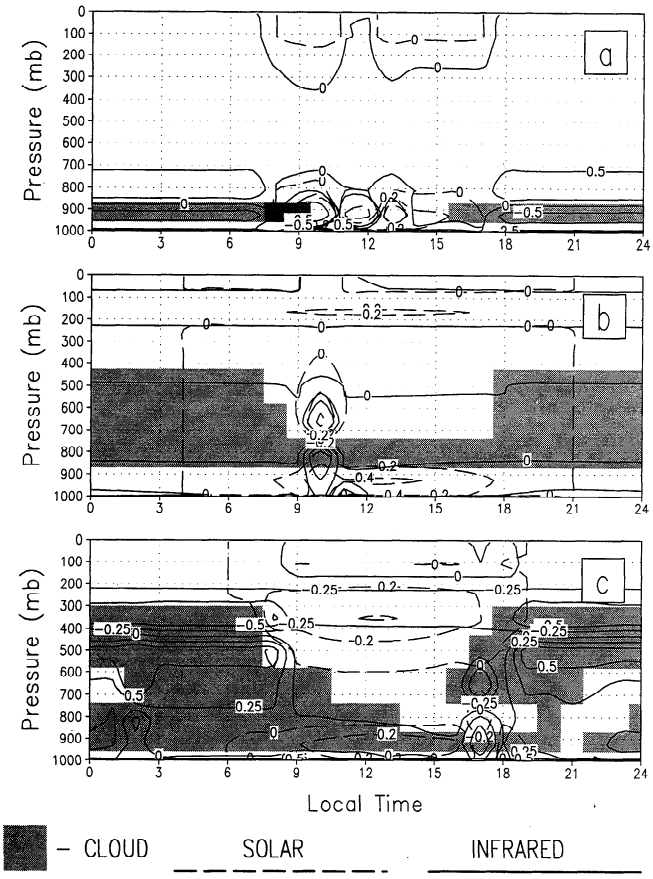

Figure 8. Final equilibrium diurnal distribution of clouds, and change of radiative heating rates due to average continental tropospheric aerosol pollution with optical depth 0.216 for (a) midlatitude winter, (b) summer, and (c) tropics spring. To compare to the control cloud distributions and heating rates, see Figure A1.

vapor feedback virtually cancels the effects of the aerosols. Nonlinear cloud feedbacks, however, substantially modify the response. In the tropics, aerosols by themselves produce warming, with a decrease of the DTR, due to the cloud feedbacks. In the summer, the clouds negate the aerosol cooling, producing essentially no temperature change. In the winter, there is enhanced cooling due to the cloud feedbacks, and an increase of the DTR, with more cooling in the morning, at the time of the minimum temperature.

Diurnal average heating in the tropics is produced by increasing of the cloud tops (Figure 8a), as in the CO_2 doubling case, but in this case it is caused by aerosol-induced solar absorption in the atmosphere and the cloud dynamical response. In the winter, the bottom of clouds is below the top of the aerosol layer, so aerosol heating is realized in a layer that is already convectively unstable, and so directly influences the clouds. In addition the surface albedo is high and the reflected upward solar flux is relatively large, causing secondary effects in the aerosol and cloudy layers. As a result in the winter, cloud changes are most dramatic (Figure 8b). In the summer (Figure 8c), clouds changed only between 0900 and 1100. IR cooling follows these cloud changes.

The changes of downward solar and IR fluxes and net change of all fluxes (including all radiative and boundary layer fluxes) for all regimes with interactive and fixed clouds are shown in Figures 9-11. Variations of clouds cause compensating short-term and diurnal mean changes of solar and IR fluxes of different signs. The interactive clouds are so dominant that fixed cloud net surface feedbacks have different shapes, phases, and even signs as compared with those from interactive clouds. In the summer and tropical cases, the aerosol solar forcing dominates in decreasing DTR. In the winter, the cloud feedback completely masks the aerosol solar effects. The much larger amplitude of the solar feedback in the tropical case with calculated clouds in comparison with the case with fixed clouds is explained by the general warming due to lifting of the cloud tops and larger absorption of solar NIR radiation in the moister atmosphere. In the midlatitude cases with interactive clouds and all fixed cloud cases, when aerosols provide diurnal average cooling, the accompanying decreasing of water vapor in the atmosphere leads to less absorption of the solar radiation and increasing downward solar flux. In winter with interactive clouds, this negative water vapor feedback dominates, and DTR is increased, but in other cases the changes of DTR is very small.

A different situation takes place in experiments with simultaneous 50% increase of CO_2 and the same aerosol pollution (Figure 7b). This combined atmospheric contamination is probably the closest to the actual current situation; the 50% increase in CO_2 produces approximately the same forcing as all increases of CO_2 plus other greenhouse gases to date. In this case, the surface warms in all regimes due to the greenhouse effect and the negative water vapor feedback cannot work. While the phasing of the response corresponds to the observations, the amplitudes are not exactly the same.

In experiments not shown here, we increased the aerosol optical depth up to 0.72 in the presence of a 50% increase in CO_2. In this case we get a cooling and the direct aerosol forcing tries to produce a decreasing of DTR (Figure 1b), but the water vapor negative feedback is so strong that even this large aerosol increase does not give a significant change of DTR.

Discussion And Conclusions

By using a sophisticated radiative-convective model of the diurnal cycle we have evaluated the effects of increased CO_2 and aerosols on the diurnal cycle of surface temperature and found that feedbacks dominate the response. In particular:

1. IR forcings contribute mainly to try to change the diurnal mean temperature, but solar forcings directly force a change of DTR.

2. Greenhouse warming produces a water vapor feedback, which causes decreasing DTR due to NIR absorption. The direct CO_2 forcing itself has a very small diurnal asymmetry.

3. Aerosol effects depend on a large number of factors in comparison with well-mixed CO_2, including vertical distribution with respect to clouds and surface albedo, so the net aerosol effect may increase or decrease DTR. Aerosol provides a strong diurnally asymmetrical primary forcing, decreasing DTR, but the accompanying decrease of temperature and water vapor mask the effect on DTR, so the DTR change itself is small and has only a weak dependence on aerosol optical depth.

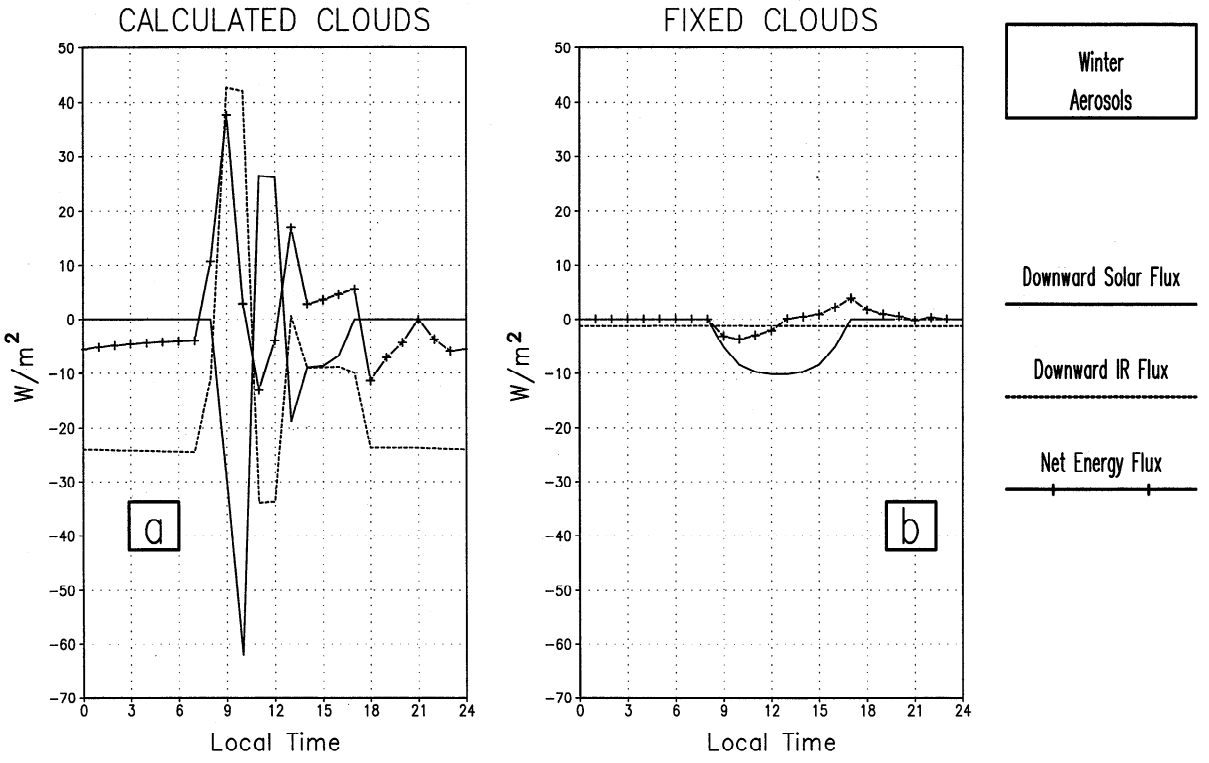

Figure 9. Changes of all surface flux components for aerosol pollution in midlatitude winter (a) for interactive clouds and (b) for fixed clouds.

4. When both CO_2 and aerosols increase, CO_2 controls the mean temperature and the aerosol solar forcing effectively decreases the DTR without a strong negative daytime water vapor-solar radiation feedback.

5. Cloud feedbacks may increase or decrease DTR and the diurnal average climate sensitivity, and therefore regional effects of clouds may be more significant than on a global average. Clouds can cause diurnal mean IR heating

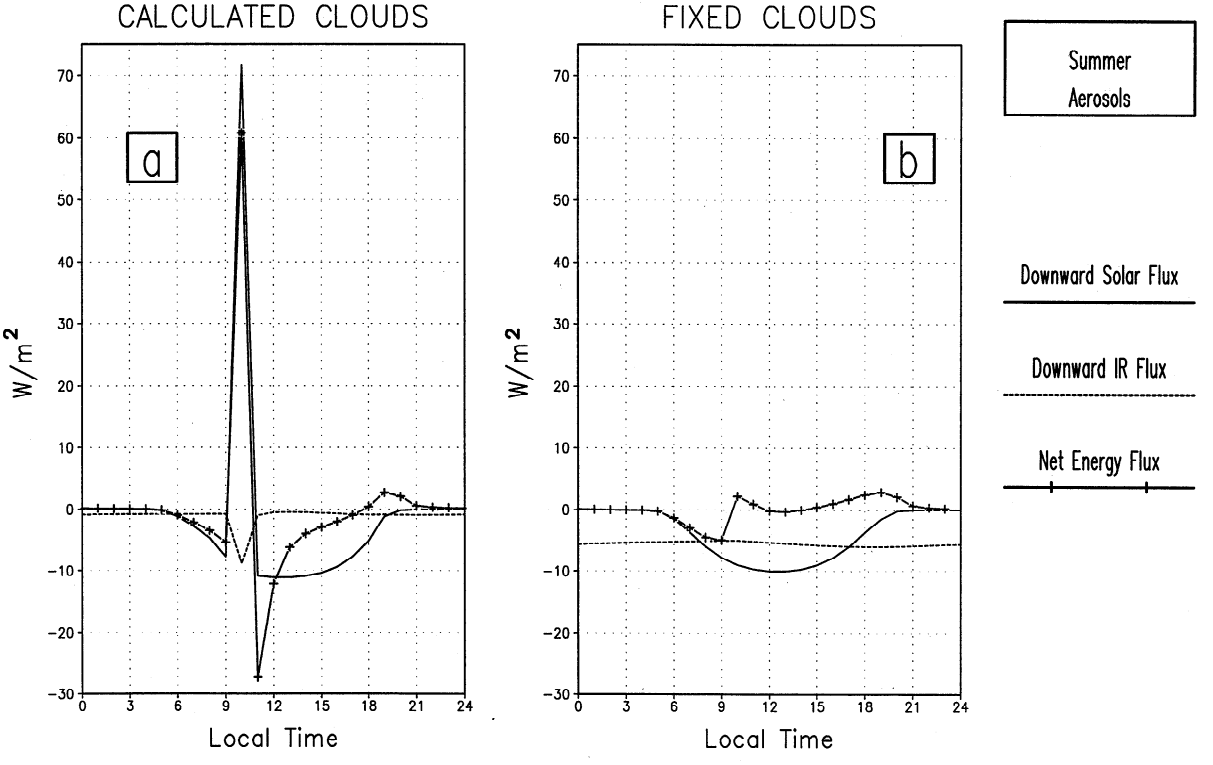

Figure 10. Same as Figure 9, but for midlatitude summer.

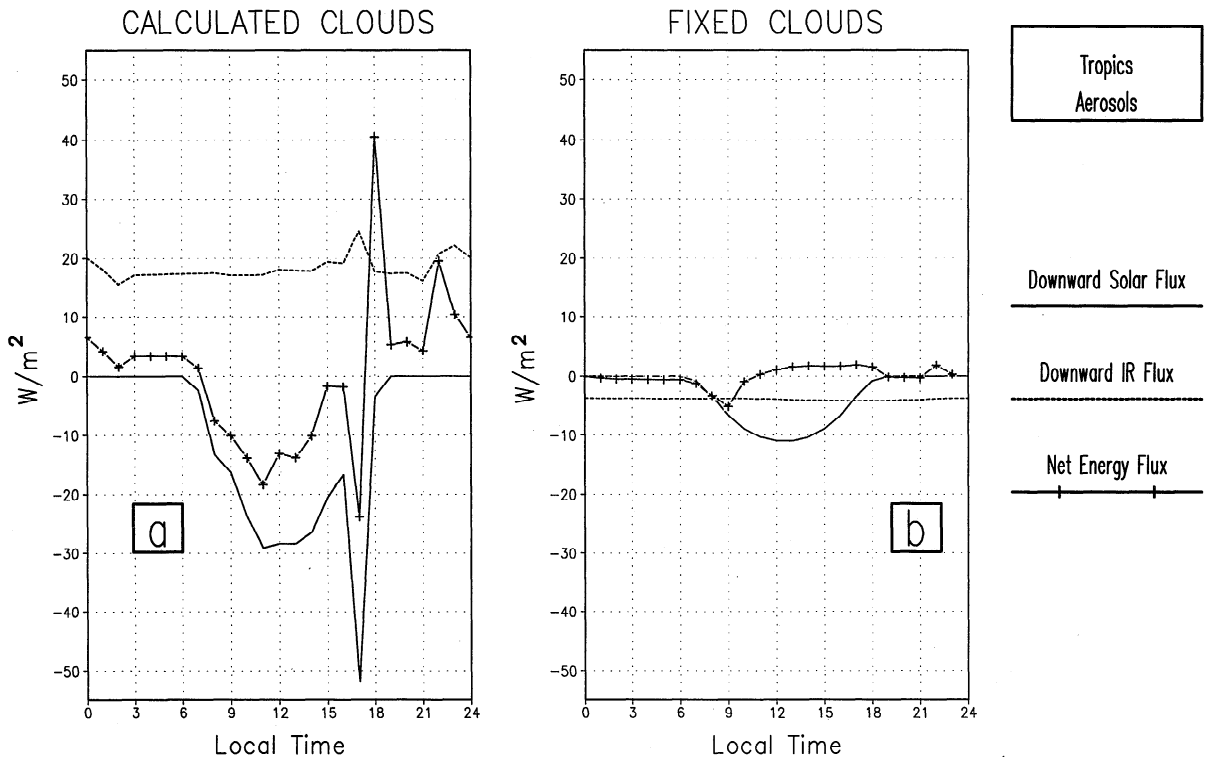

Figure 11. Same as Figure 9, but for tropics in spring.

accompanied by decreasing DTR, as in the tropics due to lifting of the cloud top, or the opposite, as in winter for the aerosol case. They also force strong short-term changes of solar and IR fluxes of opposite signs due to redistribution in time, which is observed in all cases, but is especially strong for the aerosol case in winter. The timing of these changes is very important for the evolution of DTR. In all cases the cloud contribution is not small and interactive clouds give a very different picture than for constant clouds. Therefore the improvement of cloud models, including cloud dynamics, microphysical processes, interactions with aerosol, and NIR radiative transport, is a crucial point in the quantification of the DTR change.

6. The change of large-scale flow, which can be calculated only with a GCM, may also contribute to diurnal asymmetry even if it has no significant diurnal variations. However, the shape of the diurnal oscillation and its sensitivity depends significantly on local physical processes, the description of which needs to be improved in GCMs.

Our theoretical results confirm observational evidence of a reduction of the diurnal temperature range as climate warms and the importance of cloud and water vapor feedbacks. For the most realistic case of 50% effective CO_2 increase and aerosols, the model results show diurnal asymmetry of the warming but do not exactly reproduce the observations and show more warming during the daytime than is observed at most stations (Figure 7b). Therefore it is important to point out the limitations of our study. By including CO_2 and typical aerosol forcings and prognostic water vapor and clouds, we attempt to include some of the most important processes which affect the diurnal cycle, but what we have left out may be of equal importance. This includes land surface soil moisture and biosphere feedbacks, snow/albedo feedbacks, aerosol effects on cloud microphysics, cloud ice microphysics, variable advective fluxes and vertical motion, more detailed boundary layer feedbacks, more detailed cloud distribution feedbacks, other greenhouse gases, and other aerosol types and distributions. Similarly, changing the methods we used to include the processes that we included may also affect the results. Further work will be necessary to evaluate their relevance.

Appendix: Radiative Convective Model of the Diurnal Cycle

Introduction

Radiative convective models (RCMs) are one of the basic types in the hierarchy of the climate models [*Schneider and Dickinson*, 1974; *Schlesinger and Mitchell*, 1985] and serve as the basis for the description of physical processes in general circulation models (GCMs). Traditionally, RCMs have been used to describe globally or hemispherically averaged vertical atmospheric thermal structure, when advective sources vanish due to spatial averaging. *Manabe and Strickler* [1964] and *Manabe and Wetherald* [1967] were the first to utilize RCMs to evaluate several important climatic processes. First-generation RCMs [*Ramanathan and Coakley*, 1978] have been limited by the specification of clouds, and relative or absolute humidity, as well as a simplified radiative equilibrium boundary condition for the soil.

Modifications of the RCM approach in the last decade by different authors have enriched the model physics by including a boundary layer, finite thermal capacity surface, advective sources, hydrological cycle, diurnal variations, and even cloud microphysics, but none have built a model suitable

for investigation of the diurnal cycle. *Ramanathan* [1981] developed an RCM with a boundary layer, but with prescribed clouds and relative humidity profiles. *Warrilow* [1986] and *Iacobellis and Somerville* [1991] designed models of cloud and boundary layer processes in the atmospheric column but did not try to calculate equilibrium regimes. To investigate the influence of surface properties on local climate, Warrilow allowed only small stochastic variations of the vertical moisture profiles from a prescribed profile. Iacobellis and Somerville carried out diagnostic calculations driven by observational data including advection to predict the onset of the Indian monsoon. *Betts and Ridgway* [1989] developed a specialized RCM to investigate boundary layer effects in tropics and also calculated humidity interactively. The model of *Koster and Eagleson* [1990] accounted for advective sources, calculated the transient (not equilibrium) seasonal or diurnal cycles of surface hydrology, and used a simplified description of radiative effects with fixed cloudiness and relative humidity. *Moritz and Beesley* [1992] used an RCM with a boundary layer, developed by *MacKay and Khalil* [1991], to investigate the effects of sea ice on climate. Warrilow's model with prescribed cloud amount and humidity was used in thermal equilibrium mode to investigate changes of the diurnal cycle in response to CO_2 doubling by *Cao et al.* [1992]. *Randall et al.* [1991] used a one-dimensional model with full physics and complete hydrological cycle to study the diurnal cycle of precipitation forced with prescribed advective fluxes, but gave little consideration to surface temperature variations. *Sinha and Shine* [1994] calculated clouds and cloud microphysics in their RCM, but prescribed the vertical distribution of humidity, and did not have a diurnal cycle or boundary layer. *Rennó et al.* [1994] incorporate a sophisticated cloud parameterization in an RCM accounting for cloud microphysics and an interactive hydrological cycle, but in a diurnal average mode with a zero thermal capacity swamp surface.

We combined some of the previous achievements and develop an RCM of the diurnal cycle, which is forced by prescribed advection and accounts interactively for boundary layer processes, turbulence, convection, cloudiness, and hydrological cycle, and incorporates a spectral radiative transport in a cloudy and polluted atmosphere. No previous papers have combined all these features in one model that can be used to investigate all the important local feedbacks for the diurnal cycle problem. We have already applied our model to calculate the effects of observed stratospheric aerosol, water vapor and ozone changes after the 1991 Pinatubo eruption [*Stenchikov and Robock*, 1993] and in a process study of the influence of snow cover on outgoing longwave radiation [*Groisman et al.*, 1994].

Model Description

Energy and water vapor balances. The evolution of the air temperature T and water vapor mixing ratio q are described by:

$$\frac{\partial}{\partial t}(c_p T) = \frac{g}{p_s}\frac{\partial}{\partial \sigma}(I\uparrow - I\downarrow + S\uparrow - S\downarrow + F_T^T + F_C^T) + LC \qquad \text{(A1)}$$

$$\frac{\partial q}{\partial t} = \frac{g}{p_s}\frac{\partial}{\partial \sigma}(F_T^q + F_C^q) - C \qquad \text{(A2)}$$

where

- t time;
- σ p/p_s, the vertical coordinate;
- p pressure;
- p_s surface air pressure, set to 1000 mbar here;
- c_p specific heat of air at constant pressure;
- C condensation or evaporation rate;
- $I\uparrow$ the total upward thermal flux;
- $S\uparrow$ total upward solar flux;
- $I\downarrow$ the total downward thermal flux;
- $S\downarrow$ total downward solar flux;
- $F_{T,C}^T$ turbulent and convective fluxes of internal energy;
- $F_{T,C}^q$ turbulent and convective fluxes of water vapor;
- L latent heat of vaporization;
- g acceleration due to gravity.

At the top of the atmosphere, the downward solar and thermal radiation are prescribed:

$$\sigma = 0 \qquad I\downarrow = 0 \text{ and } S\downarrow = f(\phi,t) \qquad \text{(A3)}$$

where ϕ = latitude. At the surface,

$$\sigma = 1 \qquad S\uparrow = \alpha S\downarrow, \qquad \text{(A4)}$$

where α is surface albedo. The surface radiates upward according to the Stefan-Boltzmann law, modified for a surface that is not absolutely black:

$$\sigma = 1 \qquad I\uparrow = \varepsilon \sigma T_g^4 + (1-\varepsilon) I\downarrow \qquad \text{(A5)}$$

where ε is the emissivity. At the ground, temperature T_g is defined by the energy balance relation with the soil thermal capacity c_g taken to be equal to the thermal capacity of a 10-cm water layer:

$$\text{At the ground} \qquad c_g\frac{\partial T_g}{\partial t} = S\downarrow - S\uparrow + I\downarrow - I\uparrow - F_L - F_S + Q_A \qquad \text{(A6)}$$

where F_L is latent heat flux, F_S is sensible heat flux, and Q_A is total (sensible and latent) advective source of energy.

Energy received by the atmospheric column by advection is not prescribed with a vertical distribution, but rather is absorbed by the surface, transformed in the form of latent and sensible heat, and redistributed by internal physical mechanisms, such as land-atmosphere interaction, convection, turbulence, and radiation. This procedure permits us to minimize the number of external parameters and better control the conditions in the sensitivity tests. Even with this simplification the model realistically reproduces some observed climate regimes. This procedure is analogous to placing the radiative forcing of aerosols into the surface heat budget [*Kiehl and Briegleb*, 1993] or tuning a model by varying the solar constant [*Rennó et al.*, 1994], as most of the energy change in the latter procedure is also realized at the surface.

Over land, due to conservation of energy on the average during the day, the advective sources of energy in the atmospheric column in thermal equilibrium balance the net radiation at the top of the atmosphere. This means, for

example, that the value and characteristic spatial scale of advective sources may be evaluated by the corresponding top-of-the-atmosphere radiative balance [*Peixoto and Oort*, 1992].

Radiative transport. Radiative fluxes are calculated by a spectral radiative scheme with 42 spectral bands for the range $0.125\ \mu m \le \lambda \le 250\ \mu m$ [*Prigarin et al.*, 1990]. It calculates multiple scattering of solar radiation in the visible and near-IR bands with the delta-Eddington approximation and uses different transparency functions in other bands. Optically active aerosols and all the following gases are modeled with spectrally dependent optical characteristics: H_2O, CO_2, O_3, CH_4, N_2O, CFC-11, and CFC-12. This radiation scheme is essentially the same as that of *Rozanov and Frolkis* [1986] and *Frolkis and Rozanov* [1992], which has been validated as part of the Intercomparison of Radiation Codes used in Climate Models (ICRCCM) for infrared [*Ellingson et al.*, 1991] and solar radiation [*Fouquart et al.*, 1991]. In those publications, it was referenced as the *Karol* [1986] scheme.

Convection. Convective adjustment is based on the idea of convective equilibrium [*Kelvin*, 1862]. It is less sophisticated than cumulus parameterization [*Arakawa and Schubert*, 1974; *Kuo and Raymond*, 1980] but is less sensitive and contains no empirical parameters in the moist adiabatic formulation. The effectiveness of timescaling for adjustment was demonstrated by *Betts and Miller* [1986], where the profiles were forced to adjust exponentially to a prescribed one with a prescribed characteristic time. The similar idea of soft convective adjustment was used implicitly by *Krishnamurti et al.* [1980].

The idea of parameterization of convection by threshold diffusion, developed by *Priestley* [1959] was first used for the RCM investigation of the atmospheres of Venus and Mars [*Gierasch and Goody*, 1968]. *Ramaswamy and Kiehl* [1985] applied the same formulation to investigate nuclear winter effects in the Earth's atmosphere. In both cases, however, the authors took into account only diffusion transport of internal energy without detailed treatment of water vapor lifting and condensation.

We have found a variational principle, which is equivalent to moist adiabatic adjustment and leads to a new type of threshold diffusion parameterization of convection. This parameterization treats simultaneously the transport of internal energy and water vapor, incorporating phase transformations and conserving total energy. This convective scheme does not contain new physics in comparison with moist adiabatic adjustment but accounts for the characteristic timescale of the convection, is realized in differential continuous form, and provides a new theoretical link between diffusion parameterization and adjustment.

Moist adiabatic adjustment has been widely used in RCMs and in GCMs with moderate spatial resolution. An increasing of the spatial resolution in GCMs makes possible the use of more sophisticated parameterizations, designed for a grid scale of 100-200 km. But for climatic calculations with a spatial scale of 1000 km, the physical parameterizations developed here are appropriate. We chose a scheme that is representative of the 1000-km scale, which produces a physically reasonable qualitative and quantitative picture and that is currently in use in state-of-the-art GCMs, such as the one at GFDL. Our model allows the use of more sophisticated schemes, and in the future we will test the sensitivity of our results to different convection schemes; for the purposes of this paper, we only show the qualitative importance of cloud feedbacks relative to other processes.

Variational principle for convective adjustment. Consider an atmospheric column with some vertical distribution of thermodynamic parameters and water vapor:

$$H_E = c_p T + Lq;\ H_S = H_E + gz \tag{A7}$$

where z is altitude, and H_E and H_S are the total specific energy and static energy, respectively. In accordance with the adjustment procedure in regions of instability, when the vertical gradient of temperature is high enough and the water vapor mixing ratio reaches its saturation level q_s,

$$q = q_s;\ \frac{dH_S}{d\sigma} > 0, \tag{A8}$$

convection mixes the air conservatively, that is

$$\int_0^1 H_E\, d\sigma = \text{constant} \tag{A9}$$

and

$$q = q_s(T);\ \frac{dH_S}{d\sigma} = 0. \tag{A10}$$

This produces neutral, stable vertical distributions of static energy and saturated water vapor profiles. In the unstable regions (where convection occurs), $q = q_s$, so H_S is a function only of T. Using (A8) and (A10), we can write the functional

$$Q = \int_0^1 \frac{D}{2}\left(\frac{dH_S}{d\sigma}\right)^2 d\sigma \tag{A11}$$

where $D = 0$ in the stable regions and $D = D_0 > 0$ in the regions where the atmosphere is unstable. This means that Q equals the sum of the integrals over all the unstable regions:

$$A_i < \sigma < B_i,\ i = 1, 2, 3, ... \tag{A12}$$

In these regions, we have unstable conditions ($dH_s/d\sigma > 0$) and on the boundaries

$$\sigma = A_i \text{ and } \sigma = B_i \qquad \frac{dH_S}{d\sigma} = 0. \tag{A13}$$

The functional reaches a minimum with a neutral stable distribution (A10), which is the same solution as found by *Kelvin* [1862] and as postulated by the adjustment.

Varying the functional

$$\delta Q = \sum_i \left[-\int_{A_i}^{B_i} \frac{d}{d\sigma} D \frac{dH_S}{d\sigma} \delta H_S\, d\sigma + D \frac{dH_S}{d\sigma} \delta H_S \Big|_{A_i}^{B_i} \right] = 0, \tag{A14}$$

and taking into account the boundary conditions (A13), which are the natural boundary condition for the functional, we get the condition of the extremum, or Euler equation of the functional:

$$\frac{d}{d\sigma} D \frac{dH_S}{d\sigma} = \frac{d}{d\sigma} D \left[\frac{dH_E}{d\sigma} - \frac{RT}{\sigma} \right] = 0, \tag{A15}$$

where R is the gas constant for air. Strictly speaking, this equation must be solved in all regions (A12) with boundary conditions (A13), and gives the steady solution (A9) and (A10). In the dry case (setting $L = 0$), we get the same equation used previously by *Gierasch and Goody* [1968] and *Ramaswamy and Kiehl* [1985]:

$$\frac{d}{dz}\left[\frac{p_S}{\rho g} D\left(\frac{dT}{dz}+\frac{g}{c_P}\right)\right]=0 \qquad \text{(A16)}$$

Starting from (A15), we can write the equation for a nonstationary diffusion process, which has the same steady solution as (A10) and conserves total energy in the column:

$$\frac{\partial H_E}{\partial t}=\frac{g}{p_s}\frac{\partial}{\partial \sigma}\left[\frac{g\rho^2}{p_s}K\left(\frac{\partial H_E}{\partial \sigma}-\frac{RT}{\sigma}\right)\right] \qquad \text{(A17)}$$

To get the steady solution (A9) and (A10) we need to integrate (A17) until stabilization. In nature, convection does not reach equilibrium immediately, but takes 2-3 hours. So here we have produced a convective parameterization in a nonstationary form (A17). The convective diffusion coefficient K in this formulation depends on stability, which is the solution of the equation, and is large in unstable regions and 0 in stable ones. Its characteristic value can be determined by considering the well-known convective characteristic height scale of order ΔZ = 1 km and characteristic time scale of order $\tau = 10^4$ s:

$$K = O\left(\frac{(\Delta Z)^2}{\tau}\right) = 100\,\frac{\mathrm{m}^2}{\mathrm{s}} \qquad \text{(A18)}$$

Integrating over the column with zero fluxes at the bottom and top of the atmosphere, we get the energy conservation relation:

$$\frac{d}{dt}\int_0^1 H_E\, d\sigma = 0 \qquad \text{(A19)}$$

Moist convection: In the moist, unstable cases, represented by (A8), we solve (A17) with diffusion coefficient

$$\begin{aligned} K &= 0, && \frac{\partial H_E}{\partial \sigma}-\frac{RT}{\sigma}\le 0 \\ K &= 100\,\frac{\mathrm{m}^2}{\mathrm{s}}, && \frac{\partial H_E}{\partial \sigma}-\frac{RT}{\sigma}>0 \end{aligned} \qquad \text{(A20)}$$

and boundary conditions:

$$\sigma = 0,\ 1 \qquad K\left[\frac{\partial H_E}{\partial \sigma}-\frac{RT}{\sigma}\right] = 0, \text{ since } K = 0. \qquad \text{(A21)}$$

The internal boundary conditions (A13) are realized automatically. The transport of pollutants can be incorporated in the same manner as in dry convection.

In accordance with (A19), this procedure conserves total energy. The resulting values of temperature T' and water vapor mixing ratio q' are defined from the transcendental equations:

$$\begin{aligned} c_p T' + L\, q_s(T') &= H'_E \\ q' &= q_s(T') \end{aligned} \qquad \text{(A22)}$$

where H'_E is redistributed by the convection value of the energy.

Dry convection: In dry convection there is no water phase transformation. Therefore we calculate dry convective transport using (A17), but for dry conditions. The diffusion coefficient is defined by (A20) again for dry conditions.

Clouds. Convective and layer clouds, which are generated internally by the model, play an important role in stabilizing the thermal equilibrium solution due to albedo feedback, and therefore can exert a very important influence on climate sensitivity. The fractional cover of layer clouds is taken to be 1 in layers where nonconvective condensation takes place. Convective clouds with cloud fraction 0.3 appear in the layers where convection leads to decreasing of the water vapor mixing ratio. We chose this cloud fraction as a reasonable agreement with observations. Of course, a more detailed convective parameterization could be incorporated in the model, but for our initial diurnal cycle calculations, we avoid the additional complication of convective cloud amount feedbacks. Cloud water content in cloud layers is diagnostically taken to be proportional to the saturation mixing ratio $q_s(\sigma)$. The optical characteristics of clouds are defined by the *Stephens* [1978] approximation.

Boundary layer and surface characteristics. A Richardson number dependent parameterization of the boundary layer [*Deardorff*, 1972] is used to define sensible (F_S) and latent (F_L) fluxes:

$$\begin{aligned} F_S &= \rho c_p c_d V\left(T_g - T_1\right) \\ F_L &= L\rho c_d V W_g\left(q_s\left(T_g\right) - q_1\right) \end{aligned} \qquad \text{(A23)}$$

where c_d is the drag coefficient, V surface wind, W_g ground wetness, $q_s(T_g)$ saturated specific humidity at the surface, and q_1 water vapor mixing ratio at the top of the surface layer σ = 0.991. Equation (A6) is used to calculate surface temperature.

Turbulent fluxes of internal energy and water vapor can be expressed in Reynolds' diffusion form [*Reynolds*, 1903] with a turbulent diffusion coefficient, which decreases rapidly in the free atmosphere:

$$K_T = 5\,\sigma^4. \qquad \text{(A24)}$$

The value of the turbulent diffusion coefficient can be scaled as $(\Delta Z)^2/\tau$, which corresponds to a characteristic spatial scale of order 100 m and characteristic timescale of the order of 1 hour. At the surface, the turbulent fluxes are equal to sensible and latent heat fluxes to the atmosphere from surface, and they vanish at the top of the atmosphere.

Numerics. The calculations are performed by a time-marching scheme with time step equal to 1 hour until convergence of the diurnally averaged radiative balance at the top of the atmosphere with an accuracy of 0.05 W/m^2. The vertical resolution for this model may be arbitrary, but in this version a 12-layer grid similar to the NCAR CCM1 is used for comparisons with GCM calculations.

Results

We simulated the climate for three distinct climatic regimes (midlatitude summer and winter and tropical spring), and conducted comparisons of the calculated vertical atmospheric structure and diurnal cycle with observations. Parameters of

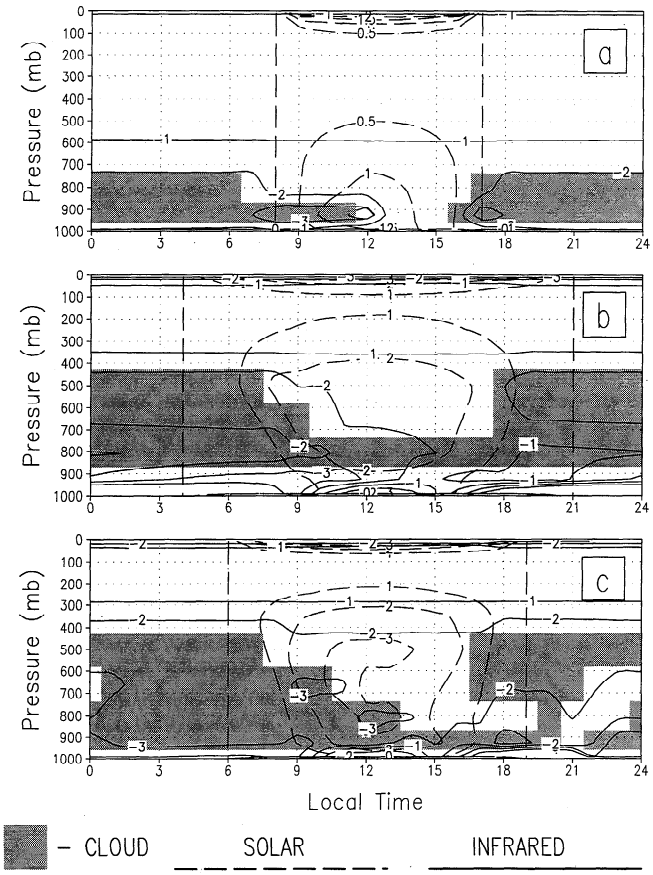

Figure A1. Diurnal cycles of solar and infrared heating rates (K/day) and convective clouds (with cloud fraction = 0.3) for the 3 cases: (a) midlatitude winter, (b) midlatitude summer, and (c) tropics in spring.

the runs are presented in Table 1. The observed atmospheric vertical profiles are retrieved from a gridded climatology based on radiosonde data and the analysis of the European Center for Medium-Range Weather Forecasts [*Dept. of Commerce and U.S. Navy*, 1993]. We averaged the data from the National Solar Radiation Data Base [*National Renewable Energy Laboratory*, 1992] for 3 years (1961-1963) to get the observed climatology of the diurnal cycle. The comparison of the observed and calculated climates shows that model is able, with the same set of internal parameters, to realistically describe different climate regimes, including vertical atmospheric thermal structure, water vapor distribution, diurnal cycles of precipitation, surface temperature, and surface fluxes of the latent and sensible heat, and cloudiness.

In Figure A1, the space-time structures of the cloud distributions and radiative heating are presented for each case. In all the cases, we have only convective clouds with cloud fraction specified to be 0.3. Diurnal changes of temperature and water vapor are significant only near the surface, but clouds and convective water transport change dramatically during the day in the entire troposphere. In all cases cloud tops are lower in the daytime, when the convective moistening of the atmosphere in all cases is the strongest. This also has important interactions with the radiative regime of the system, as the low clouds in the day reflect solar radiation and increase outgoing IR flux. In the tropics, very strong convective instability takes place at approximately 2100 as well as during the daytime. This leads to an increase of precipitation and short-term fluctuation of the surface fluxes.

Acknowledgments. We thank Tom Karl for valuable discussions. This work was supported by NASA grant NAG 5-1835 and NSF grant ATM-8920590.

References

Arakawa, A., and W. H. Schubert, Interaction of a cumulus cloud ensemble with the large-scale environment, I, *J. Atmos. Sci., 31*, 674-701, 1974.

Betts, A. K., and M. J. Miller, A new convective adjustment scheme, I: Observational and theoretical basis, *Q. J. R. Meteorol. Soc., 112*, 677-691, 1986.

Betts, A. K., and W. Ridgway, Climatic equilibrium of the atmospheric convective boundary layer over a tropical ocean, *J. Atmos. Sci., 46*, 2621-2641, 1989.

Cao, H. X., J. F. B. Mitchell, and J. R. Lavery, Simulated diurnal range and variability of surface temperature in a global climate model for present and doubled CO_2 climates, *J. Clim., 5*, 920-943, 1992.

Charlson, R. J., S. E. Schwartz, J. M. Hales, R. D. Cess, J. A. Coakley, Jr., J. E. Hansen, and D. J. Hofmann, Climate forcing by anthropogenic aerosols, *Science, 255*, 423-430, 1992.

D'Almeida, G. A., P. Koepke, and E. P. Shettle, *Atmospheric Aerosols. Global Climatology And Radiative Characteristics*, A. Deepak Publ., Hampton, Va., 1991.

Deardorff, J. W., Parameterization of the planetary boundary layer for use in general circulation models, *Mon. Weather Rev., 100*, 93-106, 1972.

Department of Commerce and U.S. Navy, Global upper air climatic atlas, CD-ROMs CDRM 1114370, CDRM 1114380, and CDRM 1114390, Washington, D.C., 1993.

Ellingson, R. G., J. Ellis, and S. Fels, The intercomparison of radiation codes used in climate models: Longwave results, *J. Geophys. Res., 96*, 8,929-8,954, 1991.

Folland, C. K., T. R. Karl, N. Nicholls, B. S. Nyenzi, D. E. Parker, K. Y. Vinnikov, Observed climate variability and change, in *Climate Change 1992, The Supplementary Report to the IPCC Scientific Assessment*, edited by J. T. Houghton, B. A. Callander, and S. K. Varney, pp. 135-170, Cambridge Univ. Press, New York, 1992.

Fouquart, Y., B. Bonnel, and V. Ramaswamy, Intercomparing shortwave radiation codes for climate studies, *J. Geophys. Res., 96*, 8,955-8,968, 1991.

Frolkis, V. A., and E. V. Rozanov, Radiation code for climate and general circulation models, paper presented at International Radiation Symposium, Tallin, Estonia, Aug. 3-8, 1992.

Gierasch, P. J., and R. Goody, A study of the thermal and dynamical structure of the Martian lower atmosphere, *Planet. Space Sci., 16*, 615-646, 1968.

Groisman, P. Y., T. R. Karl, R. W. Knight, and G. L. Stenchikov, Changes of snow cover, temperature, and radiative heat balance over the Northern Hemisphere, *J. Clim., 7*, 1633-1656, 1994.

Hansen, J., A. Lacis, R. Ruedy, M. Sato, and H. Wilson, How sensitive is the world's climate? *Natl. Geogr. Res. Explor., 9*, 142-158, 1993.

Hansen, J., M. Sato, and R. Ruedy, Long-term changes of the diurnal temperature cycle: Implications about mechanisms of global change, *Atmos. Res., 37*, 175-209, 1995.

Iacobellis, S. F., and R. C. J. Somerville, Diagnostic modeling of the Indian monsoon onset, I, Model description and validation, *J. Atmos. Sci., 48*, 1948-1959, 1991.

Karl, T. R., G. Kukla, V. N. Razuvayev, M. J. Changery, R. J. Quayle, R. R. Heim, Jr., D. R. Easterling, and C. B. Fu, Global warming: Evidence for asymmetric diurnal temperature change, *Geophys. Res. Lett., 18*, 2253-2256, 1991.

Karl, T. R., P. D. Jones, R. W. Knight, G. Kukla, N. Plummer, V. Razuvaev, K. P. Gallo, J. Lindseay, R. J. Charlson, and T. C. Peterson, Asymmetric trends of daily maximum and minimum temperature, *Bull. Am. Meteorol. Soc., 74*, 1007-1023, 1993.

Karol, I. (Ed.), *Radiative-Photochemical Models of the Atmosphere*, (in Russian), 192 pp., Hydrometeoizdat, Leningrad, 1986.

Kelvin, W. Thompson, Baron, On the convective equilibrium of temperature in the atmosphere, *Proc. Manchester Philos. Soc., VII*, 170-176, 1862.

Kiehl, J. T., and B. P. Briegleb, The relative roles of sulfate aerosols and greenhouse gases in climate forcing, *Science, 260*, 311-314, 1993.

Koster, R. D., and P. S. Eagleson, A one-dimensional interactive soil-atmosphere model for testing formulations of surface hydrology, *J. Clim., 3*, 593-606, 1990.

Krishnamurti, T. N., V. Ramanathan, H. Pan, R. J. Pasch, and J. Molonari, Cumulus parameterization and rainfall rates, I, *Mon. Weather Rev., 108*, 465-472, 1980.

Kuo, H. L., and W. H. Raymond, A quasi-one-dimensional cumulus cloud model and parameterization of cumulus heating and mixing effects, *Mon. Weather Rev., 108*, 991-1009, 1980.

Lindzen, R. S., A. Y. Hou, and B. F. Farrell, The role of the convective model choice in calculating the climate impact of doubling CO_2, *J. Atmos. Sci., 39*, 1189-1205, 1982.

MacKay, R. M., and M. A. K. Khalil, Theory and development of a one-dimensional time-dependent radiative convective climate model, *Chemosphere, 22*, 383-417, 1991.

Manabe, S., and R. F. Strickler, Thermal equilibrium of the atmosphere with a convective adjustment, *J. Atmos. Sci., 21*, 361-365, 1964.

Manabe, S., and R. T. Wetherald, Thermal equilibrium of the atmosphere with a given distribution of relative humidity, *J. Atmos. Sci., 24*, 241-259, 1967.

Moritz, R. E., and J. A. Beesley, Modeling the interactions of sea ice and climate in the central Arctic, *Proc. Third Conf. on Polar Meteorol. and Oceanogr.*, Am. Meteorol. Soc., Boston, pp. 105-108, 1992.

National Renewable Energy Laboratory, *User's Manual, National Solar Radiation Data Base (1961-1990) Version 1.0*, vol. 1, Nat. Clim. Data Cen., Asheville, N.C., 1992.

Peixoto, J. P., and A. H. Oort, *Physics of Climate*, 520 pp., Amer. Inst. of Phys., New York, 1992.

Priestley, C. H. B., *Turbulent Transfer in the Lower Atmosphere*, Univ. of Chicago Press, Chicago, 1959.

Prigarin, V. E., G. L. Stenchikov, and V. A. Frolkis, The calculation of radiative transfer in turbid and cloudy atmosphere: Description of the model (in Russian), in *Contributions on Applied Mathematics*, 14 pp., Comp. Cen. of the USSR Acad. of Sci., Moscow, 1990.

Ramanathan, V., The role of the ocean-atmosphere interactions in the CO_2 climate problem, *J. Atmos. Sci., 38*, 918-930, 1981.

Ramanathan, V., and J. A. Coakley, Jr., Climate modeling through radiative-convective models, *Rev. Geophys. Space Phys., 16*, 465-489, 1978.

Ramaswamy, V., and J. T. Kiehl, Sensitivities of the radiative forcings due to large loadings of smoke and dust aerosols, *J. Geophys. Res., 90*, 5597-5613, 1985.

Randall, D. A., Harshvardhan, and D. A. Dazlich, Diurnal variability of the hydrologic cycle in a general circulation model, *J. Atmos. Sci., 48*, 40-62, 1991.

Rennó, N. O., K. A. Emanuel, and P. H. Stone, Radiative-convective model with an explicit hydrologic cycle 1, Formulation and sensitivity to model parameters, *J. Geophys. Res., 99*, 14,429-14,441, 1994.

Reynolds, O., *Papers on Mechanical and Physical Subjects*, vol. III, *The Sub-Mechanics of the Universe*, 254 pp., Cambridge Univ. Press, New York, 1903.

Rind, D., R. Goldberg, and R. Ruedy, Change in climate variability in the 21st Century, *Clim. Change, 14*, 5-38, 1989.

Rozanov, E. V., and V. A. Frolkis, Calculations of the fields of longwave and shortwave radiation in the atmosphere (in Russian), in *Radiative-Photochemical Models of the Atmosphere*, Chap. 3, edited by I. Karol, pp. 51- 70, Hydrometeoizdat, Leningrad, 1986.

Schlesinger, M. E. and J. F. B. Mitchell, Model projections of equilibrium climatic response to increased carbon dioxide, in *Projecting the Climatic Effects of Increasing Carbon Dioxide*, Chap. 4, edited by M. C. MacCracken and F. M. Luther, pp. 81-148, Lawrence Livermore Natl. Lab., Livermore, Calif., 1985.

Schneider, S. H., and R. E. Dickinson, Climate modeling, *Rev. Geophys. Space Phys., 12*, 447-493, 1974.

Sinha, A. and K. P. Shine, A one-dimensional study of possible cirrus cloud feedbacks, *J. Clim., 7*, 158-173, 1994.

Stenchikov, G. L. and A. Robock, Climatic effects due to water vapor amount increase in the stratosphere after the Pinatubo eruption. *EOS Trans. AGU, 74* (43), Fall Meet. Suppl., 114, 1993.

Stephens, G. L., Radiation profiles in extended water clouds, II, Parameterization schemes, *J. Atmos. Sci., 35*, 2123-2132, 1978.

Veltishchev, N. N., and P. F. Demchenko, Estimation of the diurnal cycle of the greenhouse effect of CO_2 in the earth's atmosphere, *Proc. Russ. Acad. Sci., 330*, 369-371, 1993.

Warrilow, D. A., Indications of the sensitivity of European climate to land use variations using a one-dimensional model, in *Proceedings of the Conference on Parameterization of Land-Surface Characteristics; Use of Satellite Data and Climate Studies; First Results of ISLSCP*, ESA SP-248, pp. 159-166, European Space Agency, Rome, 1986.

Williamson, D. L., J. T. Kiehl, V. Ramanathan, R. E. Dickinson, and J. J. Hack, Description of NCAR Community Climate Model (CCM1), *Tech. Note TN-285+STR*, 112 pp., Natl. Cen. for Atmos. Res., Boulder, Colo., 1987.

A. Robock and G. L. Stenchikov, Department of Meteorology, University of Maryland, College Park, MD 20742. (e-mail: alan@atmos.umd.edu; gera@atmos.umd.edu)

(Received March 1, 1995; revised June 20, 1995;
accepted June 20, 1995.)